Analysis of Kinetic Isotope Effects for Proton-Coupled Electron Transfer Reactions†

Sarah J. Edwards, Alexander V. Soudackov, and Sharon Hammes-Schiffer*

Department of Chemistry, 104 Chemistry Building, Pennsylvania State University, University Park, Pennsylvania 16802

Received: October 15, 2008; Revised Manuscript Received: December 11, 2008

A series of rate constant expressions for nonadiabatic proton-coupled electron transfer (PCET) reactions are analyzed and compared. The approximations underlying each expression are enumerated, and the regimes of validity for each expression are illustrated by calculations on model systems. In addition, the kinetic isotope effects (KIEs) for a series of model PCET reactions are analyzed to elucidate the fundamental physical principles dictating the magnitude of the KIE and the dependence of the KIE on the physical properties of the system, including temperature, reorganization energy, driving force, equilibrium proton donor−acceptor distance, and effective frequency of the proton donor−acceptor mode. These calculations lead to three physical insights that are directly relevant to experimental data. First, these calculations provide an explanation for a decrease in the KIE as the proton donor−acceptor distance increases, even though typically the KIE will increase with increasing equilibrium proton donor−acceptor distance if all other parameters remain fixed. Often the proton donor−acceptor frequency decreases as the proton donor−acceptor distance increases, and these two effects impact the KIE in opposite directions, so either trend could be observed. Second, these calculations provide an explanation for an increase in the KIE as the temperature increases, even though typically the KIE will decrease with increasing temperature if all other parameters remain fixed. The combination of a rigid hydrogen bond, which corresponds to a high proton donor−acceptor frequency, and low solvent polarity, which corresponds to small solvent reorganization energy, allows the KIE to either increase or decrease with temperature, depending on the other properties of the system. Third, these calculations provide insight into the dependence of the rate constant and KIE on the driving force, which has been studied experimentally for a wide range of PCET systems. The rate constant increases as the driving force becomes more negative because excited vibronic product states associated with low free energy barriers and relatively large vibronic couplings become accessible. The ln[KIE] has a maximum near zero driving force and decreases significantly as the driving force becomes more positive or negative because the contributions from excited vibronic states increase as the reaction becomes more asymmetric, and contributions from excited vibronic states decrease the KIE. These calculations and analyses lead to experimentally testable predictions of trends in the KIEs for PCET systems.

I. Introduction

Proton-coupled electron transfer (PCET) plays an important role in a wide range of chemical and biological processes. PCET reactions involve the coupled transfer of both an electron and a proton. According to the general definition of PCET, the mechanism can be either sequential or concerted, and the electron and proton can transfer in different directions or in the same direction, either between the same sites or between different sites. This paper focuses on the broad class of PCET reactions that involve the transfer of an electron and a proton with no stable intermediate. These types of PCET reactions have been extensively studied both experimentally[1−20] and theoretically.[21−30]

The fundamental properties of PCET systems can be characterized by measuring the kinetic isotope effect (KIE), which is the ratio of the rate for hydrogen to the rate for deuterium. The experimentally observed magnitudes of the KIE, as well as the dependence of the KIE on properties such as temperature and driving force, vary widely for different PCET systems. Numerous theoretical models have been developed to describe these experimental data.[17−30] Many of these models build upon previous theoretical studies of electron transfer[31,32] and vibrationally nonadiabatic proton transfer reactions.[33−36]

In this paper, we analyze and compare a series of rate constant expressions for nonadiabatic PCET reactions. We enumerate the approximations underlying each expression and illustrate the regimes of validity for each expression through calculations on model systems. In addition, we analyze the KIEs for a series of model systems to elucidate the fundamental physical principles dictating both the magnitude of the KIE and the dependence of the KIE on the properties of the system. Specifically, we examine the impact of the proton transfer interface properties (i.e., the equilibrium proton donor−acceptor distance and the effective frequency of the proton donor−acceptor mode) on the KIE. We also study the dependence of the KIE on the solvent reorganization energy, the temperature, and the driving force. These calculations and analyses lead to physical insights that assist in the interpretation of existing experimental data and provide experimentally testable predictions of trends in the KIEs.

An outline of this paper is as follows. In Section II, we present a series of rate constant expressions and discuss the approximations underlying each expression. In Section III, we analyze these rate constant expressions by applying them to model PCET systems.

† Part of the "Max Wolfsberg Festschrift".

* To whom correspondence should be addressed. E-mail: shs@chem.psu.edu.

10.1021/jp809122y CCC: $40.75
Published on Web 01/30/2009

This analysis illustrates the regimes of validity for each rate constant expression and elucidates the dependence of the KIE on the physical properties of the system, including temperature, reorganization energy, driving force, equilibrium proton donor−acceptor distance, and effective frequency of the proton donor−acceptor mode. Section IV summarizes the new physical insights that are directly relevant to experimental data and the experimentally testable predictions provided by these calculations.

II. Theory

A. Rate Constant Expressions. In this paper, we use a series of vibronically nonadiabatic rate constant expressions that have been derived previously.[25,27] In this formulation, the PCET reaction is described in terms of nonadiabatic transitions between pairs of reactant and product mixed electron−proton vibronic states. The rate constant expressions are based on Fermi's golden rule formalism in conjunction with linear response theory for the solvent environment. For simplicity, we use the term solvent to denote both solvent and protein. The detailed derivations of these rate constant expressions are presented elsewhere. Here we simply present the final expressions and discuss the approximations underlying each expression.

In the derivations of the rate constant expressions, the nonadiabatic coupling between the reactant and product vibronic states is approximated to be of the form

$$V_{\mu\nu}(R) = V_{\mu\nu}^{(0)}\exp[-\alpha_{\mu\nu}(R-\bar{R}_\mu)] \tag{1}$$

where $\bar{R}_\mu$ is the equilibrium value of R for the reactant state μ, $V_{\mu\nu}^{(0)}$ is the vibronic coupling between reactant state μ and product state ν at distance $R = \bar{R}_\mu$, and $\alpha_{\mu\nu}$ is the exponential decay parameter. This form of the coupling is a reasonable approximation in the region of R near its equilibrium value.[37] In the electronically nonadiabatic limit for proton transfer, the vibronic coupling is of the form $V_{\mu\nu}(R) = V^{el}S_{\mu\nu}(R)$, where V^{el} is the electronic coupling and $S_{\mu\nu}(R)$ is the overlap between the reactant and product proton vibrational wave functions for states μ and ν at a distance R.[30,38] In this limit, $V_{\mu\nu}^{(0)} = V^{el}S_{\mu\nu}^{(0)}$ in eq 1, where $S_{\mu\nu}^{(0)}$ is the overlap at the distance $\bar{R}_\mu$ and the parameter $\alpha_{\mu\nu}$ describes the approximately exponential decay of the overlap with R near $\bar{R}_\mu$.

Using the short-time, high-temperature approximation for the solvent modes and representing the R-mode time correlation function by that of a quantum mechanical harmonic oscillator, the rate constant can be expressed as:[27]

$$k^{quant} = \sum_\mu P_\mu \sum_\nu \frac{|V_{\mu\nu}^{(0)}|^2}{\hbar^2\Omega}\exp\left[\frac{2\lambda_{\mu\nu}^{(\alpha)}\zeta}{\hbar\Omega}\right]\times \int_{-\infty}^{\infty} d\tau\ \exp\left[-\frac{1}{2}\chi\tau^2 + p(\cos\tau - 1) + i(q\sin\tau + \theta\tau)\right] \tag{2}$$

with the dimensionless parameters defined as

$$\zeta = \coth\left(\frac{1}{2}\beta\hbar\Omega\right);\ \chi = \frac{2\lambda}{\beta\hbar^2\Omega^2};\ \theta = \frac{\Delta G_{\mu\nu}^0 + \lambda}{\hbar\Omega}$$
$$p = \zeta\frac{\lambda_{\mu\nu}^{(\alpha)}}{\hbar\Omega};\ q = \frac{\lambda_{\mu\nu}^{(\alpha)}}{\hbar\Omega} \tag{3}$$

Here the summations are over reactant and product vibronic states, $\beta = 1/k_BT$, P_μ is the Boltzmann probability for the reactant state μ, λ is the solvent reorganization energy, $\Delta G_{\mu\nu}^0$ is the free energy of reaction for states μ and ν, $\lambda_{\mu\nu}^{(\alpha)}$ is the coupling reorganization energy defined as $\lambda_{\mu\nu}^{(\alpha)} = \hbar^2\alpha_{\mu\nu}^2/2M$, and M and Ω are the R-mode effective mass and frequency, respectively. The free energy of reaction is often expressed as $\Delta G_{\mu\nu}^0 = \Delta G^0 + \Delta\varepsilon_{\mu\nu}$, where $\Delta G^0 \equiv \Delta G_{00}^0$ and $\Delta\varepsilon_{\mu\nu}$ is the difference between the product and reactant vibronic energy levels ν and μ relative to their respective ground states. The short-time, high-temperature approximation for the solvent is valid when the solvent reorganization energy λ is large enough to ensure that the dynamics of the solvent fluctuations are fast on the time scale of the coherent nonadiabatic transitions. These expressions also assume that the solvent reorganization energy is the same for all pairs of reactant/product vibronic states and that the equilibrium proton donor−acceptor distance is the same for all reactant and product states. Furthermore, the inner-sphere reorganization energy for the intramolecular solute modes can be added to the solvent reorganization energy in the high-temperature (low-frequency) limit for these modes.[25,39−41] These approximations are valid for the majority of homogeneous PCET systems of interest, and eq 2 will be used as a benchmark for the more approximate methods discussed below.

This rate constant expression can be simplified in certain limiting regimes pertaining to the R-mode frequency. In the high-temperature (low-frequency) limit for the R mode ($\hbar\Omega \ll k_BT$), the rate constant has the form[27,42]

$$k^{highT} = \sum_\mu P_\mu \sum_\nu \frac{|V_{\mu\nu}^{(0)}|^2}{\hbar}\exp\left[\frac{2k_BT\alpha_{\mu\nu}^2}{M\Omega^2}\right]\sqrt{\frac{\pi}{(\lambda+\lambda_{\mu\nu}^{(\alpha)})k_BT}}\times \exp\left[-\frac{(\Delta G_{\mu\nu}^0 + \lambda + \lambda_{\mu\nu}^{(\alpha)})^2}{4(\lambda+\lambda_{\mu\nu}^{(\alpha)})k_BT}\right] \tag{4}$$

This high-temperature rate constant expression is derived from eq 2 by performing a short-time expansion of the trigonometric functions up to second order and evaluating the time integral analytically.

In the low-temperature (high-frequency) limit for the R mode ($\hbar\Omega \gg k_BT$), the rate constant has the form:[27]

$$k^{lowT} = \sum_\mu P_\mu \sum_\nu \frac{|V_{\mu\nu}^{(0)}|^2}{\hbar}\sqrt{\frac{\pi}{\lambda k_BT}}\exp\left[\frac{\hbar\alpha_{\mu\nu}^2}{2M\Omega}\right]\times \exp\left[-\frac{(\Delta G_{\mu\nu}^0 + \lambda)^2}{4\lambda k_BT}\right] \tag{5}$$

This low-temperature rate constant expression is derived from eq 2 using the stationary phase method and is valid only in the strong solvation regime (i.e., $\lambda > |\Delta G_{\mu\nu}^0|$ for all relevant pairs of states). An equivalent expression can be obtained by averaging the squared vibronic coupling over the ground-state vibrational wave function of the R-mode earlier in the derivation.

An alternative rate constant expression attributed to Kutznetsov and Ulstrup[33] has been implemented by Klinman and others to study PCET reactions in enzymes.[19,20] This expression is based on the Marcus theory rate constant for nonadiabatic electron transfer modified by the inclusion of R-dependent Franck−Condon overlap terms for the transferring hydrogen, thermally averaged over a Boltzmann distribution for R. This expression is of the form

$$k^{UK} = \sum_\mu P_\mu \sum_\nu \frac{|V^{el}|^2}{\hbar}\sqrt{\frac{\pi}{\lambda k_BT}}\times \exp\left[-\frac{(\Delta G_{\mu\nu}^0 + \lambda)^2}{4\lambda k_BT}\right]\int_0^\infty P(R)[S_{\mu\nu}(R)]^2 dR \tag{6}$$

where $P(R) = \sqrt{M\Omega^2/2\pi k_BT}\exp[-M\Omega^2(R-\bar{R})^2/(2k_BT)]$ is the Boltzmann probability for a classical harmonic oscillator

representation of the *R*-mode. Note that the normalization constant for the Boltzmann probability assumes integration over all values of *R*; this assumption is reasonable because *P(R)* is negligible for negative values of *R*. The Marcus theory rate constant for nonadiabatic electron transfer with the Franck−Condon overlap terms is based on the treatment of an intramolecular solute mode quantum mechanically in the low-temperature (high-frequency) limit, and this solute mode is assumed to be uncoupled from the solvent.[39−41] Thus, eq 6 is based on the reasonable assumption that the proton vibrational frequency is in the high-frequency regime relative to the thermal energy, as well as the additional assumption that the proton motion is not coupled to the solvent. Furthermore, the thermal averaging procedure with the classical Boltzmann probability used in eq 6 is valid only in the high-temperature (low-frequency) limit for the *R*-mode.

The rate constants k^{UK} and k^{highT} become identical when the vibronic coupling is assumed to be the product of an electronic coupling and the proton vibrational wave function overlap (i.e., $V_{\mu\nu} = V^{el}S_{\mu\nu}$), the overlap is assumed to decrease exponentially with *R* near its equilibrium value (i.e., $S_{\mu\nu} = S_{\mu\nu}^{(0)}\exp[-\alpha_{\mu\nu}(R - \bar{R}_{\mu})]$), and $\lambda_{\mu\nu}^{(\alpha)} \ll \lambda$.[43] Since $\lambda_{\mu\nu}^{(\alpha)}$ is inversely proportional to the mass *M* corresponding to the *R*-mode, the difference between k^{UK} and k^{highT} is smaller for larger *M*. Note that both of these rate constant expressions are strictly valid only in the low-frequency regime for the *R*-mode, where $\hbar\Omega \ll k_B T$.

B. Kinetic Isotope Effects. In the high-temperature (low-frequency) regime for the *R*-mode, the KIE has a simple form if the reorganization energy and driving force are independent of isotope, only the ground reactant and product vibronic states contribute to the rates, and $\lambda_{\mu\nu}^{(\alpha)} \ll \lambda$. In this case, the KIE is of the form[44]

$$\mathrm{KIE} \approx \frac{|S_H|^2}{|S_D|^2}\exp\left[-\frac{2k_B T}{M\Omega^2}(\alpha_D^2 - \alpha_H^2)\right] \quad (7)$$

where S_H and S_D represent the overlaps of the hydrogen and deuterium ground state wave functions, and α_H and α_D represent the exponential dependence of these overlaps on *R*. The temperature dependence of the KIE can be analyzed from the derivative of the ln[KIE] with respect to temperature:

$$\frac{d}{dT}\ln[\mathrm{KIE}] \approx -\frac{2k_B}{M\Omega^2}(\alpha_D^2 - \alpha_H^2) \quad (8)$$

The simple expressions in eqs 7 and 8 enable the analysis of qualitative trends pertaining to the magnitude and temperature dependence of the KIE, but we emphasize that they are valid only when excited vibronic states do not contribute to the rates and in the low-frequency regime for the *R*-mode.

For all of the rate constant expressions given above, the KIE depends strongly on the equilibrium *R* value and the frequency Ω of the *R*-mode. Equations 7 and 8 can be used to examine qualitative trends when only the ground reactant and product vibronic states contribute to the rates in the low-frequency regime for the *R*-mode. In this case, eq 7 indicates that the KIE is proportional to the ratio of the overlaps for hydrogen and deuterium. These overlaps are depicted in Figure 1a for Morse potentials representing the reactant and product proton potential energy curves. This figure illustrates that the hydrogen overlap is greater than the deuterium overlap for the same value of *R*. In general, the overlap between the reactant and product vibrational wave functions decreases as *R* increases for both hydrogen and deuterium. However, the overlap decreases much faster with *R* for deuterium than for hydrogen due to the larger mass of deuterium, so this ratio becomes larger as *R* increases. Figure 1b illustrates these effects for the ground reactant and product vibrational wave functions in Figure 1a. Thus, if all other quantities remain the same, the KIE increases as the equilibrium *R* value increases. Moreover, since the overlap decreases faster with *R* for deuterium than for hydrogen, $\alpha_D > \alpha_H$, and the overall quantity in the exponential of eq 7 is negative. Therefore, if all other quantities remain the same, the magnitude of the KIE will increase as the frequency Ω increases. The physical basis for this trend is that a higher frequency typically does not enable effective sampling of smaller distances.

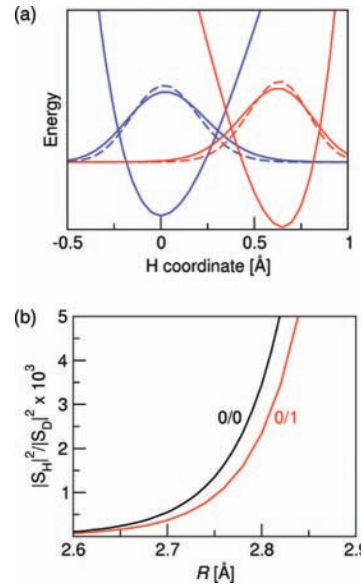

Figure 1. (a) Proton potential energy curves and the associated hydrogen (solid) and deuterium (dashed) vibrational wave functions for the ground reactant (blue) and product (red) states. The proton potential energy curves are Morse potentials with the parameters given in the text. The proton donor−acceptor distance is 2.7 Å. (b) Square of the ratio of the hydrogen and deuterium overlaps for the ground reactant and product vibrational states 0/0 (black) and the ground reactant and first excited product states 0/1 (red) as functions of the proton donor−acceptor distance *R*. Note that $(S_H/S_D)^2$ increases dramatically as *R* increases and is significantly smaller for the 0/1 pair of states.

The inclusion of excited vibronic states will influence these general trends. Figure 1b also depicts the ratio of overlaps for the ground reactant and first excited product vibrational states. For excited vibrational states, the overlap is greater, and therefore the ratio of hydrogen to deuterium wave function overlaps is smaller, than for the ground reactant and product vibrational states. In addition, the excited states often contribute more for deuterium than for hydrogen because the splittings between the energy levels are smaller for deuterium. Thus, contributions from excited vibronic states tend to decrease the magnitude of the KIE.

To analyze the temperature dependence of the KIE, we focus on the ln[KIE] because this quantity is directly related to the difference in the apparent activation energies for deuterium and hydrogen transfer. Specifically, the derivative of ln[KIE] with respect to the inverse temperature is proportional to $E_D - E_H$, where E_D and E_H are the apparent activation energies for deuterium and hydrogen transfer, respectively (i.e., E_H is proportional to the derivative of $\ln[k_H]$ with respect to inverse temperature). Equation 8 indicates that the ln[KIE] will decrease with temperature in the high-temperature (low-frequency) limit for the *R*-mode with only the ground vibronic states contributing.

Moreover, the temperature dependence of ln[KIE] will increase as the frequency Ω decreases in this regime. A more detailed analysis of these trends will be presented below by calculations on model systems.

We will also analyze the dependence of the rate constant and KIE on the driving force ΔG^0. For this purpose, we derive an approximate expression for the KIE in the vicinity of $\Delta G^0 = 0$ in the high-temperature (low-frequency) limit for the *R*-mode, assuming again that the reorganization energy and driving force are independent of isotope and that only the ground reactant and product vibronic states contribute to the rates. Performing a Taylor series of ln $[k_H^{highT}]$ and ln $[k_D^{highT}]$ about $\Delta G^0 = 0$ and retaining terms up to second order in ΔG^0 leads to:

$$\ln\left(\frac{k_L^{highT}}{k_L^0}\right) = -\frac{\Delta G^0}{2k_BT} - \frac{(\Delta G^0)^2}{4(\lambda+\lambda_\alpha^L)k_BT} \tag{9}$$

where k_L^0 with L = H or D is the high-temperature rate constant for hydrogen or deuterium, respectively, at $\Delta G^0 = 0$ and λ_α^L with L = H or D denotes $\lambda_{00}^{(\alpha)}$ for hydrogen or deuterium, respectively. Equation 9 leads to the following approximate forms of ln[KIE] and KIE:

$$\ln[\mathrm{KIE}] = \ln[\mathrm{KIE}^0] - \frac{(\Delta G^0)^2(\lambda_\alpha^D - \lambda_\alpha^H)}{4k_BT(\lambda+\lambda_\alpha^H)(\lambda+\lambda_\alpha^D)} \tag{10}$$

$$\mathrm{KIE} = \mathrm{KIE}^0 \exp\left[-\frac{(\Delta G^0)^2(\lambda_\alpha^D - \lambda_\alpha^H)}{4k_BT(\lambda+\lambda_\alpha^H)(\lambda+\lambda_\alpha^D)}\right] \tag{11}$$

where KIE^0 is the KIE evaluated at $\Delta G^0 = 0$:

$$\mathrm{KIE}^0 = \frac{|S_H|^2}{|S_D|^2}\exp\left[-\frac{2k_BT}{M\Omega^2}(\alpha_D^2 - \alpha_H^2)\right]\sqrt{\frac{\lambda+\lambda_\alpha^D}{\lambda+\lambda_\alpha^H}}\exp\left[\frac{\lambda_\alpha^D - \lambda_\alpha^H}{4k_BT}\right] \tag{12}$$

Equation 11 differs from eq 7 because the derivation of eq 11 is not based on the assumption that $\lambda_{00}^{(\alpha)} = 0$, which was assumed in the derivation of eq 7. As will be shown below, the contributions from excited vibronic states can lead to qualitative deviations from the quadratic behavior in eqs 9 and 10, particularly for the rate constant. A similar analysis was performed previously for vibrationally nonadiabatic proton transfer reactions.[45,46] Note that this driving force dependence of the KIE will not be evident using the k^{UK} rate constant expression given in eq 6.

The preceding analyses of the dependence of the KIE on temperature and driving force are based on the rate constant expression in the high-temperature (low-frequency) regime for the *R*-mode. In the low-temperature (high-frequency) regime for the *R*-mode, the KIE obtained from eq 5 including contributions from only the ground reactant and product vibronic states is:

$$\mathrm{KIE}^{lowT} = \frac{S_H^2}{S_D^2}\exp\left[-\frac{\hbar(\alpha_D^2 - \alpha_H^2)}{2M\Omega}\right] \tag{13}$$

As in the high-temperature regime, the magnitude of the KIE will increase as the equilibrium *R* value and the frequency Ω increase. In this low-temperature regime, however, the KIE is independent of both temperature and driving force when only ground states contribute. As shown below, contributions from excited vibronic states can lead to temperature dependence of the KIE in the low-temperature regime for the *R*-mode.

III. Model Calculations and Discussion

A. Model System. In this section, we analyze the rate constant expressions given above by calculating the rates and KIEs for model PCET systems. For simplicity, the reactant and product proton potential energy curves are described by Morse potentials of the form

$$E_{XY} = D_{XY}(1 - e^{-\beta_{XY}(R_{XY} - R_{XY}^o)})^2 \tag{14}$$

In all model systems studied in the present paper, the proton is assumed to transfer from a carbon atom to an oxygen atom. Thus, the Morse potential for the reactant corresponds to a C−H vibrational mode, and the Morse potential for the product corresponds to an O−H vibrational mode. We chose parameters that are typical for these types of vibrational modes.[44] The values for the dissociation energies D_{CH} and D_{OH} were chosen to be 77 and 82 kcal/mol, and the values of R_{CH}^o and R_{OH}^o were chosen to be 1.09 and 0.96 Å. The values for parameters β_{CH} and β_{OH} were chosen to be 2.068 and 2.442 $Å^{-1}$ to reproduce the typical C−H and O−H frequencies of 2900 and 3500 cm^{-1}. These Morse parameters may be varied to describe other vibrational modes, but the qualitative trends discussed below will not be significantly altered. The other parameters in the rate constant expressions are varied in these model systems. Unless otherwise stated, $M = 100$ amu, $\lambda = 30$ kcal/mol, $\Delta G^0 = -5$ kcal/mol, $T = 303$ K, $\Omega = 150$ cm^{-1}, and $\bar{R} = 2.7$ Å.

The hydrogen and deuterium vibrational wave functions are calculated by solving a one-dimensional Schrödinger equation for the hydrogen or deuterium moving in the reactant and product Morse potentials. Analytical solutions are available for the eigenfunctions of Morse potentials.[47] The Morse potentials and corresponding hydrogen and deuterium wave functions are depicted in Figure 1a. In this model, the Morse potentials are positioned so that the minima are separated by a distance of $\bar{R} - R_{CH}^o - R_{OH}^o$. The overlaps $S_{\mu\nu}^{(0)}$ between the reactant and product vibrational wave functions at $\bar{R}$ are calculated numerically. The parameters $\alpha_{\mu\nu}$ are determined for each pair of vibronic states by calculating the numerical derivatives of the natural logarithm of the corresponding overlap integrals with respect to *R* at $\bar{R}$. For $\bar{R} = 2.7$ Å, $\alpha_{00} = 17.80$ $Å^{-1}$ and 24.79 $Å^{-1}$ for hydrogen and deuterium, respectively. These values vary slightly with $\bar{R}$: at $\bar{R} = 2.8$ Å, $\alpha_{00} = 19.77$ $Å^{-1}$ and 27.47 $Å^{-1}$ for hydrogen and deuterium, respectively. These values also vary slightly for different pairs of states: at $\bar{R} = 2.7$ Å, $\alpha_{01} = 15.55$ $Å^{-1}$ and 22.58 $Å^{-1}$ for hydrogen and deuterium, respectively.

B. Comparison of rate constant expressions. As discussed above, the rate constant k^{quant} in eq 2 is valid for all frequency regimes of the *R*-mode, whereas k^{highT} in eq 4 is valid only in the high-temperature (low-frequency) limit for the *R*-mode, and k^{lowT} in eq 5 is valid only in the low-temperature (high-frequency) limit for the *R*-mode. Figure 2a depicts the dependence of the KIE on the frequency Ω of the *R*-mode for all three of these rate constant expressions. This figure illustrates that k^{highT} agrees well with k^{quant} for low *R*-mode frequencies, and k^{lowT} agrees well with k^{quant} for high *R*-mode frequencies. As discussed above, the simple KIE in eq 7 predicts the increase of the KIE as the frequency increases for the high-temperature limit of the *R*-mode. From a physical perspective, the KIE increases as the frequency increases because a higher frequency limits the ability of the system to sample smaller *R* values, and larger *R* values are associated with greater KIEs.

Figure 2b depicts the dependence of the KIE on the temperature for two different *R*-mode frequencies, $\Omega = 150$ cm^{-1} and $\Omega = 850$ cm^{-1}, with equilibrium *R* values of $\bar{R} = 2.7$ and 2.6 Å, respectively. For the lower *R*-mode frequency, the

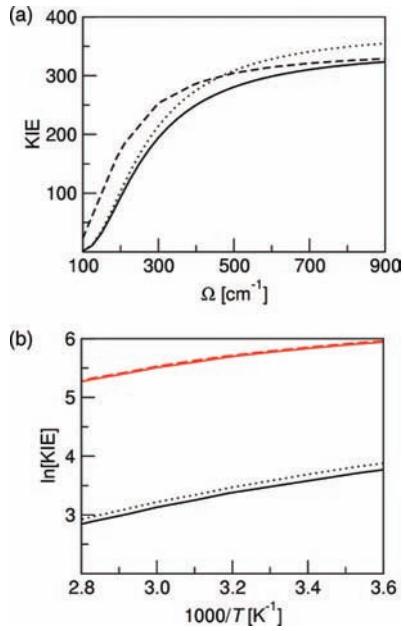

Figure 2. (a) KIE as a function of proton donor−acceptor mode frequency Ω for $\bar{R} = 2.7$ Å at $T = 303$ K calculated with k^{quant} (solid), k^{highT} (dotted), and k^{lowT} (dashed) for a model system with $\lambda = 30$ kcal/mol, $\Delta G^0 = -5$ kcal/mol, and $M = 100$ amu. (b) KIE as a function of 1000/T for $\Omega = 150$ cm^{-1} and $\bar{R} = 2.7$ Å obtained with k^{quant} and k^{highT} (black, lower curves) and for $\Omega = 850$ cm^{-1} and $\bar{R} = 2.6$ Å obtained with k^{quant} and k^{lowT} (red, upper curves). The line types are the same as in (a), and the two upper curves are virtually indistinguishable.

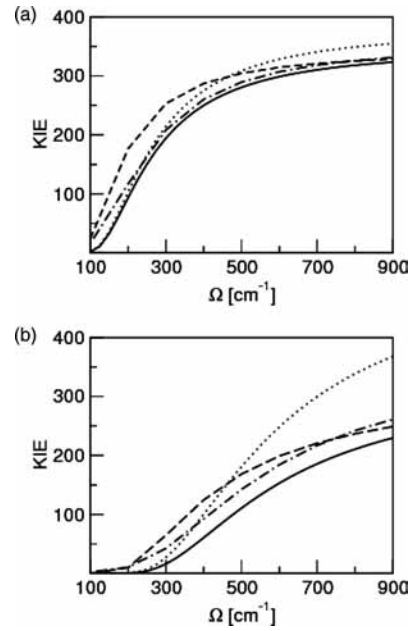

Figure 3. KIE as a function of frequency calculated with k^{quant} (solid), k^{highT} (dotted), k^{lowT} (dashed), and k^{UK} (dot-dashed) for a model system with $\lambda = 30$ kcal/mol, $\Delta G^0 = -5$ kcal/mol, $\bar{R} = 2.7$ Å, $T = 303$ K, and (a) $M = 100$ amu and (b) $M = 20$ amu.

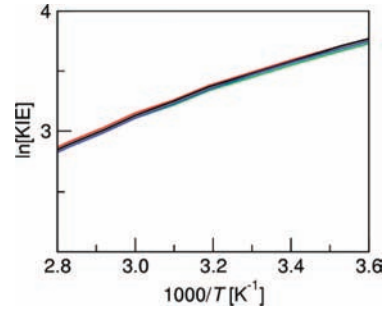

Figure 4. KIE calculated with k^{quant} for a model system with $\bar{R} = 2.7$ Å, $\Omega = 150$ cm^{-1}, $M = 100$ amu, and $\Delta G^0 = -5$ kcal/mol for different values of the reorganization energy λ. In units of kcal/mol, $\lambda = 10$ (green), 20 (red), 30 (black), and 40 (blue). The four curves are virtually indistinguishable.

temperature dependence of the KIE is similar using k^{quant} and k^{highT}. For the higher R-mode frequency, the temperature dependence of the KIE is similar using k^{quant} and k^{lowT}. A comparison of Figures 2a and 2b illustrates that decreasing $\bar{R}$ from 2.7 to 2.6 Å for $\Omega = 850$ cm^{-1} significantly decreases the KIE, mainly due to the decrease in the ratio of the hydrogen and deuterium overlaps. Typically a higher-frequency R-mode is associated with a stronger hydrogen bond, which would have a smaller equilibrium R value and therefore a lower KIE.

Figure 3 compares the KIE calculated using the rate constant k^{UK} to the KIE calculated using the rate constants k^{quant}, k^{highT}, and k^{lowT}. As discussed above, k^{UK} and k^{highT} become identical when $\lambda_{\mu\nu}^{(\alpha)} = 0$ and the overlap decays exponentially with R near its equilibrium value. Figure 3a depicts the frequency dependence of the KIE for all of these rate constant expressions with $M = 100$ amu. The KIEs obtained from k^{quant} and k^{highT} converge to the same value at low frequencies, but the KIE obtained from k^{UK} approaches a different value at low frequencies. This discrepancy arises because k^{quant} and k^{highT} are based on the assumption that the vibronic coupling decreases exponentially with R, which is valid only near the equilibrium R value, and a smaller frequency enables sampling of a wider range of R values. Although not shown in this figure, the KIEs obtained from k^{UK} and k^{highT} with $\lambda_{\mu\nu}^{(\alpha)} = 0$ are virtually identical at high frequencies, where R is nearly fixed to its equilibrium value. Furthermore, the KIEs obtained from k^{highT} with $\lambda_{\mu\nu}^{(\alpha)} = 0$ agree with those calculated using k^{quant} in the high-frequency R-mode limit because the expression for k^{highT} given in eq 4 becomes similar to the expression for k^{lowT} given by eq 5 in this limit. Figure 3b depicts the same curves as Figure 3a with $M = 20$ amu. Similar trends are exhibited in both figures, but the discrepancies between k^{quant} and both k^{highT} and k^{UK} are more pronounced for the smaller effective mass because of the larger $\lambda_{\mu\nu}^{(\alpha)}$.

C. Dependence of KIE on System Properties. In this subsection, we examine the dependence of the KIE on the physical properties of the system. First we investigate the impact of the reorganization energy λ on the magnitude and temperature dependence of the KIE. These results were calculated using the rate constant expression given in eq 2. Figure 4 indicates that the KIEs are virtually identical for reorganization energies in the range of 10−40 kcal/mol. The magnitude of the KIE does not change monotonically as λ is increased because of changes in the relative contributions from excited states.

Excited vibronic states often contribute significantly to the overall rate of PCET reactions. Given the reorganization energy and the driving force, we can generate the standard parabolic Marcus free energy curves as functions of a collective solvent coordinate.[31,32] Figure 5 depicts these free energy curves, as well as the reactant and product proton potential energy curves and associated proton vibrational wave functions, for the lowest three reactant and product vibronic states. Note that the energy splittings between the ground and excited vibronic states are determined by the energy splittings of the proton vibrational states in the Morse potentials for the reactant and product states. For reasons discussed above, the contributions of excited

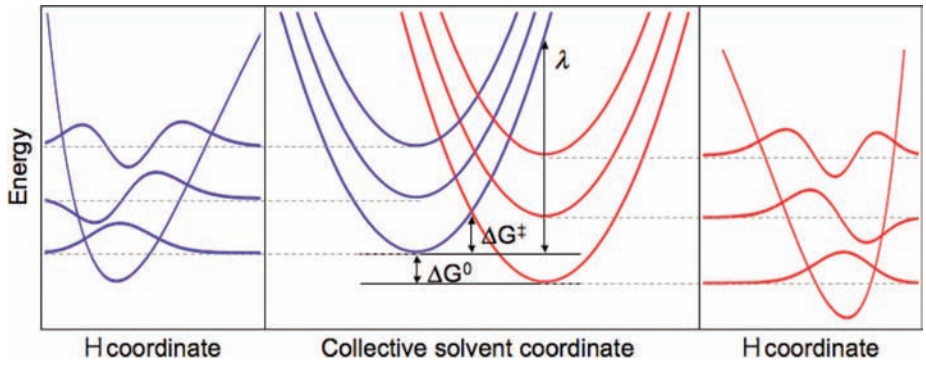

Figure 5. Free energy curves as functions of a collective solvent coordinate (center frame) with the proton potential energy curves and associated hydrogen vibrational wave functions on the left (reactant) and right (product) for a model system with $\lambda = 30$ kcal/mol and $\Delta G^0 = -5$ kcal/mol. The lowest three reactant vibronic states are shown in blue, and the lowest three product vibronic states are shown in red. The splittings between the free energy curves correspond to the splittings between the proton vibrational energy levels for the Morse potentials. The reorganization energy λ, driving force ΔG^0, and free energy barrier $\Delta G^{\ddagger}_{00}$ for the ground reactant and product vibronic states are identified.

TABLE 1: Analysis of the Contributions of Pairs of Reactant/Product Vibronic States μ/ν for a Model System with $\lambda = 30$ kcal/mol, $\bar{R} = 2.7$ Å, $M = 100$ amu, $\Omega = 150$ cm^{-1}, and $T = 303$ K[a]

ΔG^0	isotope	μ	ν	contribution to rate (%)	P_μ	$\Delta G^0_{\mu\nu}$	$\Delta G^{\ddagger}_{\mu\nu}$	$\exp[-\beta\Delta G^{\ddagger}_{\mu\nu}]$	$\lvert S^{(0)}_{\mu\nu}\rvert^2$
−5	H	0	0	96.59	0.999996	−5.00	5.21	1.75×10^{-4}	1.82×10^{-6}
		0	1	1.05	0.999996	2.53	8.82	4.36×10^{-7}	5.59×10^{-5}
		1	0	0.68	0.000004	−14.10	2.11	3.03×10^{-2}	6.80×10^{-5}
		1	1	0.03	0.000004	−6.76	4.57	5.03×10^{-4}	1.30×10^{-3}
	D	0	0	79.47	0.999875	−5.00	5.21	1.75×10^{-4}	3.27×10^{-9}
		0	1	10.31	0.999875	−0.41	7.71	2.76×10^{-6}	1.50×10^{-7}
		1	0	7.63	0.000125	−11.56	2.39	9.03×10^{-3}	1.86×10^{-7}
		1	1	1.90	0.000125	−6.15	4.74	3.80×10^{-4}	6.15×10^{-6}
0	H	0	0	95.72	0.999996	0.00	7.50	3.89×10^{-6}	1.82×10^{-6}
		0	1	0.30	0.999996	7.53	11.74	3.42×10^{-9}	5.59×10^{-5}
		1	0	1.89	0.000004	−9.10	3.64	2.37×10^{-3}	6.80×10^{-5}
		1	1	0.02	0.000004	−1.57	6.37	1.39×10^{-5}	1.30×10^{-3}
	D	0	0	77.56	0.999875	0.00	7.50	3.89×10^{-6}	3.27×10^{-9}
		0	1	4.10	0.999875	5.41	10.45	2.91×10^{-8}	1.50×10^{-7}
		1	0	15.62	0.000125	−6.56	4.58	4.97×10^{-4}	1.86×10^{-7}
		1	1	1.58	0.000125	−1.15	6.94	9.91×10^{-6}	6.15×10^{-6}
5	H	0	0	92.07	0.999996	5.00	10.21	4.34×10^{-8}	1.82×10^{-6}
		0	1	0.08	0.999996	12.53	15.07	1.34×10^{-11}	5.59×10^{-5}
		1	0	5.13	0.000004	−4.10	5.59	9.32×10^{-5}	6.80×10^{-5}
		1	1	0.02	0.000004	3.43	9.31	1.92×10^{-7}	1.30×10^{-3}
	D	0	0	66.01	0.999875	5.00	10.21	4.34×10^{-8}	3.27×10^{-9}
		0	1	1.42	0.999875	10.41	13.61	1.53×10^{-10}	1.50×10^{-7}
		1	0	27.88	0.000125	−1.56	6.74	1.37×10^{-5}	1.86×10^{-7}
		1	1	1.15	0.000125	3.85	9.55	1.29×10^{-7}	6.15×10^{-6}

[a] Free energies are given in units of kcal/mol.

vibronic states tend to decrease the KIE because the overlaps between excited vibrational wave functions are larger than the overlap between the ground reactant and product proton vibrational wave functions.

The qualitative analysis of the contributions from excited vibronic states is simplified by using the high-temperature rate constant expression given in eq 4. The relative contribution of each pair of reactant/product vibronic states is determined by a balance among the Boltzmann probability P_μ for the reactant state, the vibronic coupling $V^{(0)}_{\mu\nu} = V^{el}S^{(0)}_{\mu\nu}$, and the free energy barrier $\Delta G^{\ddagger}_{\mu\nu} = (\Delta G^0_{\mu\nu}+\lambda+\lambda^{(\alpha)}_{\mu\nu})^2/4(\lambda+\lambda^{(\alpha)}_{\mu\nu})$. The reorganization energy λ, driving force ΔG^0, and free energy barrier $\Delta G^{\ddagger}_{\mu\nu}$ for the ground reactant and product vibronic states are depicted in Figure 5. The free energy barrier contributes a factor of $\exp[-\Delta G^{\ddagger}_{\mu\nu}/k_BT]$ to the rate constant for each pair of reactant/product vibronic states. The Boltzmann probability strongly favors the ground reactant state. The vibronic coupling favors excited vibronic states because the overlaps are greater for excited-state proton vibrational wave functions. In the normal Marcus regime, the free energy barrier favors the ground product state when the reaction initiates from the ground reactant state. The relative contributions of the pairs of reactant/product vibronic states are determined from a complex interplay among these various factors.

We examined the contributions from the excited vibronic states for three model systems with $\Delta G^0 = -5$, 0, and +5 kcal/mol. The detailed analysis of the various terms for both hydrogen and deuterium is provided in Table 1. For all three model systems, the ground vibronic states dominate for hydrogen, and excited vibronic states contribute much more for deuterium. This difference can be understood in the context of Figure 6, which depicts the free energy curves for hydrogen and deuterium. In this figure, the ground vibronic states are chosen to be at the same energies for hydrogen and deuterium, but the first excited vibronic states are lower for deuterium than for hydrogen. As a result, the free energy barrier for the (0/1) pair of vibronic states (i.e., the pair corresponding to the ground reactant and first excited product state) is lower for deuterium

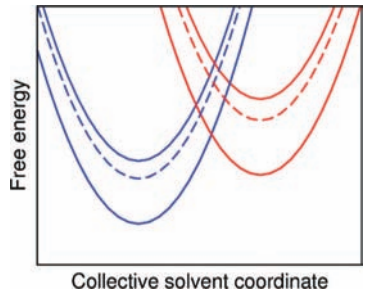

Figure 6. Free energy curves as functions of a collective solvent coordinate for hydrogen (solid) and deuterium (dashed) for a model system with $\lambda = 30$ kcal/mol and $\Delta G^0 = 5$ kcal/mol. The lowest two reactant and the lowest two product states are shown for both hydrogen and deuterium. Since the ground reactant state is chosen to have the same absolute energy for hydrogen and deuterium, the ground reactant and product states for deuterium exactly overlay those for hydrogen and therefore are not distinguishable.

than for hydrogen, leading to a greater contribution from this pair of states for deuterium. In addition, the Boltzmann probability for the first excited reactant state is significantly greater for deuterium than for hydrogen, leading to a greater contribution from the (1/0) pair of vibronic states for deuterium. The contributions from excited vibronic states are greater for the model system with $\Delta G^0 = 5$ kcal/mol, leading to a lower KIE.

We emphasize that the excited reactant states may contribute significantly to the overall PCET rate. For these model systems, the excited reactant state contributes significantly for deuterium. Although the Boltzmann probability is small for this excited state, the free energy barrier is significantly lower for the (1/0) pair of reactant/product vibronic states than for the (0/0) pair of reactant/product vibronic states. This difference in free energy barriers for the (0/0) and (1/0) pairs of reactant/product vibronic states is evident in Figure 6. In addition, the vibronic coupling is larger for the excited states. For the model system with $\Delta G^0 = 5$ kcal/mol, the first excited reactant state contributes 28% to the overall rate for deuterium. Thus, in practice, the rate constant expressions should be converged with respect to the numbers of both reactant and product vibronic states.

As discussed above, the magnitude and temperature dependence of the KIE are primarily dictated by the equilibrium proton donor−acceptor distance $\bar{R}$ and the R-mode vibrational frequency Ω. This dependence can be analyzed in the context of eqs 7 and 8 corresponding to the KIE and the derivative of the ln[KIE] with respect to the temperature. The curves in Figure 7 are calculated using the full form of the rate constant given in eq 2, and the approximate forms in eqs 7 and 8 are used only for the purposes of analysis. Figure 7a depicts the temperature dependence of the ln[KIE] for $\bar{R} = 2.7$ and 2.8 Å and $\Omega = 140$ and 180 cm^{-1}. For a fixed frequency of $\Omega = 140$ cm^{-1}, the magnitude of the KIE increases as $\bar{R}$ increases from 2.7 to 2.8 Å because the ratio of the hydrogen and deuterium overlaps in eq 7 increases. For a fixed $\bar{R}$ value of 2.7 Å, the magnitude of the KIE increases as Ω increases, as predicted by eq 7. This trend is physically reasonable because the higher frequency restricts the value of R to larger values corresponding to a greater ratio of the hydrogen and deuterium overlaps. In addition, the temperature dependence of the ln[KIE] decreases as Ω increases for fixed $\bar{R}$, as predicted by eq 8. This trend is more evident in Figure 7b, which depicts the temperature dependence of the ln[KIE] for $\bar{R} = 2.7$ and $\Omega = 150$ and 300 cm^{-1}, because the difference in frequencies is greater.

Furthermore, the equilibrium R value and the proton donor−acceptor frequency cannot usually be varied independently when designing experimental systems. Typically the frequency will increase as the equilibrium R value decreases because the hydrogen bond is stronger for shorter distances. When the frequency varies even slightly, the KIE could be observed to either increase or decrease as $\bar{R}$ increases. For example, Figure 7a depicts a comparison of two systems in which $\bar{R} = 2.7$ Å and $\Omega = 180$ cm^{-1} for the first system and $\bar{R} = 2.8$ Å and $\Omega = 140$ cm^{-1} for the second system. As shown in this figure, the first system has a higher KIE for higher temperatures, while the second system has a higher KIE for lower temperatures. This range of temperatures is close enough to room temperature to be experimentally accessible for many systems. From the experimental perspective, the KIE could be observed to increase or decrease with $\bar{R}$, depending on the temperature, change in frequency, and other characteristics of the system.

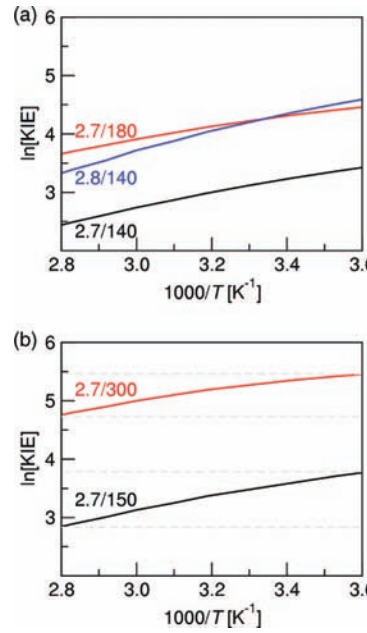

Figure 7. KIE calculated with k^{quant} for a model system with $\lambda = 30$ kcal/mol, $\Delta G^0 = -5$ kcal/mol, and $M = 100$ amu. (a) $\bar{R} = 2.7$ Å and $\Omega = 140$ cm^{-1} (black), $\bar{R} = 2.7$ Å and $\Omega = 180$ cm^{-1} (red), and $\bar{R} = 2.8$ Å and $\Omega = 140$ cm^{-1} (blue). (b) $\bar{R} = 2.7$ Å and $\Omega = 150$ cm^{-1} (black), $\bar{R} = 2.7$ Å and $\Omega = 300$ cm^{-1} (red). The curves are labeled according to the $\bar{R}/\Omega$ values in units of Å and cm^{-1}.

We emphasize that the general trends based on the analysis of eqs 7 and 8 will not always be followed. As discussed above, excited vibronic states often contribute significantly to the overall PCET rate, but eqs 7 and 8 are based on the assumption that only the ground vibronic states are contributing. Since the contributions from excited states depend on a complex interplay among several factors, including the Boltzmann probability, the vibronic coupling, and the free energy barrier, the relative contributions will vary with temperature and will differ for hydrogen and deuterium. In this case, the temperature dependence of the KIE is determined by summing over all pairs of states for hydrogen, summing over all pairs of states for deuterium, and subsequently taking the ratio of these two rate constants. In addition, eqs 7 and 8 are only valid in the high-temperature (low-frequency) regime for the R-mode. For systems that are not in the high-temperature or low-temperature regime, we must use eq 2 to evaluate the rate constants for hydrogen and deuterium, and the prediction of general qualitative trends is more difficult.

In some cases, the KIE has been observed experimentally to increase with temperature.[15] For the rate constant expressions

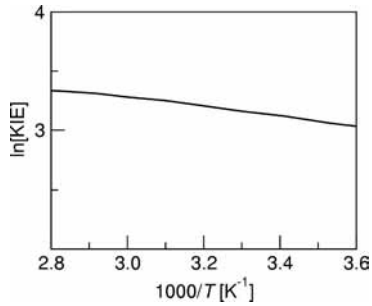

Figure 8. Temperature dependence of the KIE calculated with k^{quant} for a model system with $\lambda = 3$ kcal/mol, $\Delta G^0 = -6.5$ kcal/mol, $\bar{R} = 2.7$ Å, $\Omega = 600$ cm^{-1}, and $M = 100$ amu.

in the high-temperature (low-frequency) limit for the *R*-mode (i.e., eqs 4 and 6), the KIE tends to decrease with temperature because of the exponential prefactor that depends on temperature, as evident in eq 7. Even accounting for contributions from excited vibronic states does not seem to reverse this qualitative trend. On the other hand, for the more general rate constant expression given in eq 2, the KIE will increase with temperature for certain choices of parameters. Figure 8 depicts the temperature dependence of the KIE determined from eq 2 for a system with $\lambda = 3$ kcal/mol, $\Delta G^0 = -6.5$ kcal/mol, and $\Omega = 600$ cm^{-1}. This system is in the low-temperature (high-frequency) regime for the *R*-mode and therefore corresponds to a PCET system with a strong, rigid hydrogen bond. This system is also in the Marcus inverted region, where $-\Delta G^0 > \lambda$. The reorganization energy is quite low, corresponding to a reaction occurring in a solvent with low dielectric constant. An analysis of this model system indicates that the (0/0) and (0/1) pairs of reactant/product vibronic states contribute 71 and 29%, respectively, for hydrogen, and the (0/0) and (0/1) pairs of reactant/product vibronic states contribute 6 and 91%, respectively, for deuterium, with the remaining contributions arising from other pairs of states. A detailed analysis of a specific system exhibiting this type of temperature dependence of the KIE will be discussed elsewhere.[48]

Finally, we analyze the dependence of the rate constant and KIE on the driving force ΔG^0. Figure 9 depicts the dependence of the rate constant and the corresponding ln[KIE] on driving force for a model system with $\lambda = 20$ kcal/mol. These curves were generated using the expression for k^{highT} given in eq 4, converging the results with respect to the number of reactant and product vibronic states. For comparison, Figure 9 also depicts the results when only the ground reactant and product vibronic states are included. For the analysis, we refer to eqs 9 and 10, which are approximate forms of the rate constant and ln[KIE] including only ground reactant and product vibronic states. We emphasize that the curves in Figure 9 are calculated using the full form of the rate constant given in eq 4, and the approximate forms in eqs 9 and 10 are used only for the purposes of analysis. Figure 9 illustrates the quadratic dependence of the rate constant and ln[KIE] on the driving force when only the ground reactant and product vibronic states are included. In this case, the rate constant exhibits a maximum at $-\Delta G^0 = \lambda + \lambda_{00}^{(\alpha)}$, and the ln[KIE] exhibits a maximum at $\Delta G^0 = 0$. Since $\lambda = 20$ kcal/mol in this model system, the curvature is so small for ln[KIE] that the quadratic dependence of ln[KIE] on driving force is barely visible when only the ground states are included.

When excited vibronic states are included, however, the qualitative behavior of both the rate constant and ln[KIE] is altered. The rate constant does not decrease as ΔG^0 becomes more negative because excited vibronic product states associated with low free energy barriers and relatively large vibronic couplings become accessible. For this reason, Figure 9a exhibits an increase in the rate constant as the driving force becomes more negative. The KIE also exhibits qualitatively different behavior when excited vibronic states are included. Typically the contributions from excited vibronic states increase as ΔG^0 becomes more positive or more negative (i.e., as the reaction becomes more asymmetric). Figure 9c illustrates that the (0/0) pair dominates at $\Delta G^0 \approx 0$, the (1/0) pair dominates as the reaction becomes more endergonic, and the (2/0) pair dominates as the reaction becomes even more endergonic. Similarly, the (0/1) pair dominates as the reaction becomes more exergonic, and the (0/2) pair dominates as the reaction becomes even more exergonic. As discussed above and illustrated in Figure 1b, the KIE tends to decrease as the contributions of excited vibronic states increase because the excited vibronic states are associated with larger overlaps and therefore a smaller ratio of hydrogen to deuterium overlaps. As a result, the ln[KIE] decreases more rapidly for both positive and negative driving forces when excited vibronic states are included. Figure 9b illustrates this phenomenon for the model system studied. Note that the

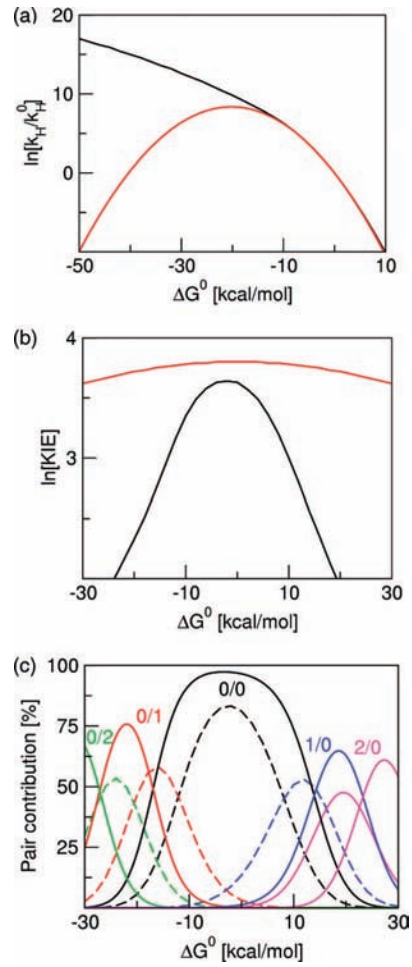

Figure 9. Driving force dependence of (a) the rate constant $k_{\text{H}}^{\text{highT}}$, (b) the associated KIE, and (c) the contributions of pairs of reactant/product vibronic states for a model system with $\lambda = 20$ kcal/mol, $\bar{R} = 2.7$ Å, $\Omega = 150$ cm^{-1}, $M = 100$ amu, and $T = 303$ K. In (a) and (b), the red curve corresponds to the calculation including only the ground reactant and product vibronic states, and the black curve corresponds to the calculation that is converged with respect to excited vibronic states. In (c), the color code for the pairs of reactant/product vibronic states is as follows: 0/0 (black), 1/0 (blue), 2/0 (magenta), 0/1 (red), and 0/2 (green).

maximum of ln[KIE] is not at exactly $\Delta G^0 = 0$ because the proton transfer interface is asymmetric (i.e., different Morse potentials are used for reactant and product states). For this model, the ground-state contributions are greatest for slightly negative driving forces due to the complex interplay of various factors in the rate constant expression. Qualitatively similar behavior is observed in the high-frequency regime for the *R*-mode using k^{lowT}. In this regime, the KIE is rigorously independent of driving force when only the ground reactant and product vibronic states are included, as indicated by eq 13, but the KIE depends on driving force in a similar manner as shown in Figure 9b when excited vibronic states are included.

Similar behavior of the KIE was observed previously for vibrationally nonadiabatic proton transfer (PT) reactions.[45,46] An important difference between vibrationally nonadiabatic PT and the PCET reactions discussed here is that typically vibrationally nonadiabatic PT is electronically adiabatic (i.e., the reaction occurs on the electronic ground state). In contrast, the PCET reactions discussed here are electronically nonadiabatic and occur on two different electronic surfaces corresponding to the two electron transfer states. As a result, the nature of the nonadiabatic coupling is different for these two types of reactions.[38] In addition, the solvent reorganization is typically much smaller for PT than for PCET because the proton is transferred a shorter distance than the electron. This difference in solvent reorganization energies leads to qualitative differences in the dependence of the KIE on driving force, particularly when only the ground states contribute to the rates.

IV. Conclusions

In this paper, we have compared the KIEs obtained with different rate constant expressions for PCET reactions. The KIEs obtained from rate constants k^{highT} and k^{lowT} rigorously approach those obtained from k^{quant} in the low-frequency and high-frequency *R*-mode limits, respectively. The KIEs obtained from the rate constant k^{UK} behave qualitatively similar to those obtained from k^{highT} and k^{quant} in the low-frequency *R*-mode regime. Analytical expressions for the dependence of the KIE on both temperature and driving force were derived including only the ground reactant and product vibronic states.

While these simple analytical expressions are useful for predicting general trends, our calculations have illustrated the importance of converging the rate constants with respect to the numbers of both reactant and product vibronic states. Excited vibronic state contributions are typically greater for deuterium than for hydrogen and decrease the magnitude of the KIE because of the smaller ratio of the hydrogen to deuterium overlaps for excited states. Although the excited reactant vibronic state has a smaller Boltzmann probability than the ground state, the free energy barrier and coupling terms may be large enough to result in a significant contribution from the excited reactant state. Moreover, the inclusion of a sufficient number of product vibronic states is particularly important when studying the driving force dependence of the KIE for very negative driving forces.

In addition, we analyzed the dependence of the magnitude of the KIE on the physical properties of the PCET system. Typically the magnitude of the KIE increases as the equilibrium proton donor−acceptor distance increases if all other parameters remain fixed. Moreover, typically the magnitude of the KIE increases as the proton donor−acceptor mode frequency increases if all other parameters remain fixed. In experimentally studied systems, often the proton donor−acceptor mode frequency increases as the equilibrium *R* value decreases, however, leading to the possibility of observing the KIE to either increase or decrease with the equilibrium *R* value. The magnitude of the KIE is relatively insensitive to changes in the solvent reorganization energy within a physically reasonable range.

Furthermore, we studied the dependence of the KIE on the temperature. In the low-frequency regime for the *R*-mode, the KIE decreases as the temperature is increased, and the temperature dependence of the ln[KIE] typically decreases as the proton donor−acceptor mode frequency increases. In the high-frequency regime for the *R*-mode, the KIE is independent of the temperature when only the ground reactant and product vibronic states contribute to the rates, but contributions from excited vibronic states could lead to either an increase or a decrease of the KIE with temperature.

We also studied the dependence of the rate constant and the KIE on the driving force. In contrast to the inverted Marcus region behavior predicted and observed experimentally for electron transfer, our calculations indicate that the PCET nonadiabatic rate constant increases as the driving force becomes more negative because excited vibronic product states associated with low free energy barriers and relatively large vibronic couplings become accessible. Moreover, the ln[KIE] is a maximum near zero driving force and decreases significantly as the driving force becomes more positive or negative because the contributions from excited vibronic states increase as the reaction becomes more asymmetric, and contributions from excited vibronic states decrease the KIE.

These calculations provide physical insights that are directly relevant to experimental data. For example, recently the magnitude of the KIE was observed experimentally to decrease with increasing proton donor−acceptor distance in phenol-base complexes, where the proton donor−acceptor distance was increased by structural modification.[49] Our calculations suggest a possible explanation for this observation in terms of a decrease in the proton donor−acceptor frequency as the proton donor−acceptor distance increases. These two effects impact the KIE in opposite directions, and the KIE may be observed to decrease with increasing proton donor−acceptor distance when the lower frequency dominates the observed trend. In another set of experiments, the KIE for the PCET reaction associated with oxidation of a ubiquinol analogue in acetonitrile was observed to increase as the temperature increases.[15] Our calculations provide an explanation for this observation in terms of a rigid hydrogen bond, which corresponds to a high proton donor−acceptor frequency, in conjunction with the low dielectric constant of acetonitrile, which corresponds to small solvent reorganization energy. These two properties allow the possibility of this type of unusual temperature dependence.[48] Finally, the dependence of the rate constant and KIE on the driving force has been studied experimentally for a wide range of PCET systems.[11,50−52] Our model calculations provide a theoretical framework for the interpretation of these types of experimental studies. Overall, these calculations on model systems assist in the interpretation of experimental data and provide predictions of trends in the KIE that can be tested experimentally.

Acknowledgment. We thank Michelle Ludlow for helpful discussions and suggesting parameters for Figure 8. We are grateful for support from NIH grant GM56207 and NSF Grant No. CHE-07-49646.

References and Notes

(1) Malmstrom, B. G. *Acc. Chem. Res.* **1993**, *26*, 332.
(2) Tommos, C.; Tang, X.-S.; Warncke, K.; Hoganson, C. W.; Styring, S.; McCracken, J.; Diner, B. A.; Babcock, G. T. *J. Am. Chem. Soc.* **1995**, *117*, 10325.

(3) Hoganson, C. W.; Lydakis-Simantiris, N.; Tang, X.-S.; Tommos, C.; Warncke, K.; Babcock, G. T.; Diner, B. A.; McCracken, J.; Styring, S. *Photosynth. Res.* **1995**, *47*, 177.
(4) Roberts, J. A.; Kirby, J. P.; Nocera, D. G. *J. Am. Chem. Soc.* **1995**, *117*, 8051.
(5) Reece, S. Y.; Nocera, D. G. *J. Am. Chem. Soc.* **2005**, *127*, 9448.
(6) Rosenthal, J.; Nocera, D. G. *Acc. Chem. Res.* **2007**, *40*, 543.
(7) Irebo, T.; Reece, S. Y.; Sjodin, M.; Nocera, D. G.; Hammarstrom, L. *J. Am. Chem. Soc.* **2007**, *129*, 15462.
(8) Sjodin, M.; Styring, S.; Akermark, B.; Sun, L.; Hammarstrom, L. *J. Am. Chem. Soc.* **2000**, *122*, 3932.
(9) Sjodin, M.; Irebo, T.; Utas, J. E.; Lind, J.; Merenyi, G.; Akermark, B.; Hammarstrom, L. *J. Am. Chem. Soc.* **2006**, *128*, 13076.
(10) Binstead, R. A.; Meyer, T. J. *J. Am. Chem. Soc.* **1987**, *109*, 3287.
(11) Fecenko, C. J.; Thorp, H. H.; Meyer, T. J. *J. Am. Chem. Soc.* **2007**, *129*, 15098.
(12) Huynh, M. H.; Meyer, T. J. *Chemical Reviews* **2007**, *107*, 5004.
(13) Mayer, J. M. *Annu. Rev. Phys. Chem.* **2004**, *55*, 363.
(14) Rhile, I. J.; Mayer, J. M. *J. Am. Chem. Soc.* **2004**, *126*, 12718.
(15) Cape, J. L.; Bowman, M. K.; Kramer, D. M. *J. Am. Chem. Soc.* **2005**, *127*, 4208.
(16) Stubbe, J.; Nocera, D. G.; Yee, C. S.; Chang, M. C. Y. *Chem. Rev.* **2003**, *103*, 2167.
(17) Roth, J. P.; Lovel, S.; Mayer, J. M. *J. Am. Chem. Soc.* **2000**, *122*, 5486.
(18) Roth, J. P.; Yoder, J. C.; Won, T.-J.; Mayer, J. M. *Science* **2001**, *294*, 2524.
(19) Knapp, M. J.; Rickert, K. W.; Klinman, J. P. *J. Am. Chem. Soc.* **2002**, *124*, 3865.
(20) Meyer, M. P.; Klinman, J. P. *Chem. Phys.* **2005**, *319*, 283.
(21) Cukier, R. I. *J. Phys. Chem.* **1994**, *98*, 2377.
(22) Cukier, R. I. *J. Phys. Chem.* **1996**, *100*, 15428.
(23) Cukier, R. I.; Nocera, D. G. *Ann. Rev. Phys. Chem.* **1998**, *49*, 337.
(24) Soudackov, A.; Hammes-Schiffer, S. *J. Chem. Phys.* **1999**, *111*, 4672.
(25) Soudackov, A.; Hammes-Schiffer, S. *J. Chem. Phys.* **2000**, *113*, 2385.
(26) Hammes-Schiffer, S. *Acc. Chem. Res.* **2001**, *34*, 273.
(27) Soudackov, A.; Hatcher, E.; Hammes-Schiffer, S. *J. Chem. Phys.* **2005**, *122*, 014505.
(28) Siebrand, W.; Smedarchina, Z. *J. Phys. Chem. B* **2004**, *108*, 4185.
(29) Mincer, J. S.; Schwartz, S. D. *J. Chem. Phys.* **2004**, *120*, 7755.
(30) Georgievskii, Y.; Stuchebrukhov, A. A. *J. Chem. Phys.* **2000**, *113*, 10438.
(31) Marcus, R. A. *Ann. Rev. Phys. Chem.* **1964**, *15*, 155.
(32) Marcus, R. A.; Sutin, N. *Biochim. Biophys. Acta* **1985**, *811*, 265.
(33) Kuznetsov, A. M.; Ulstrup, J. *Can. J. Chem.* **1999**, *77*, 1085.
(34) Borgis, D.; Lee, S.; Hynes, J. T. *Chem. Phys. Lett.* **1989**, *162*, 19.
(35) Borgis, D.; Hynes, J. T. *J. Chem. Phys.* **1991**, *94*, 3619.
(36) Warshel, A.; Chu, Z. T. *J. Chem. Phys.* **1990**, *93*, 4003.
(37) Hatcher, E.; Soudackov, A.; Hammes-Schiffer, S. *Chem. Phys.* **2005**, *319*, 93.
(38) Skone, J. H.; Soudackov, A. V.; Hammes-Schiffer, S. *J. Am. Chem. Soc.* **2006**, *128*, 16655.
(39) Kestner, N. R.; Logan, J.; Jortner, J. *J. Phys. Chem.* **1974**, *78*, 2148.
(40) Bixon, M.; Jortner, J. *Adv. Chem. Phys.* **1999**, *106*, 35.
(41) Ulstrup, J.; Jortner, J. *J. Chem. Phys.* **1975**, *63*, 4358.
(42) Hammes-Schiffer, S.; Soudackov, A. V. *J. Phys. Chem. B* **2008**, *112*, 14108–14123.
(43) Hammes-Schiffer, S.; Hatcher, E.; Ishikita, H.; Skone, J. H.; Soudackov, A. V. *Coord. Chem. Rev.* **2008**, *252*, 384.
(44) Hatcher, E.; Soudackov, A. V.; Hammes-Schiffer, S. *J. Am. Chem. Soc.* **2007**, *129*, 187.
(45) Kiefer, P. M.; Hynes, J. T. *J. Phys. Chem. A* **2004**, *108*, 11793.
(46) Kiefer, P. M.; Hynes, J. T. *J. Phys. Chem. A* **2004**, *108*, 11809.
(47) Dahl, J. P.; Springborg, M. *J. Chem. Phys.* **1987**, *88*, 4535.
(48) Ludlow, M.; Soudackov, A. V.; Hammes-Schiffer, S. to be submitted.
(49) Markle, T. F.; Mayer, J. M. Personal communication.
(50) Fecenko, C. J.; Meyer, T. J.; Thorp, H. H. *J. Am. Chem. Soc.* **2006**, *128*, 11020.
(51) Markle, T. F.; Rhile, I. J.; DiPasquale, A. G.; Mayer, J. M. *Proc. Natl. Acad. Sci. U.S.A.* **2008**, *105*, 8185.
(52) Sjodin, M.; Styring, S.; Wolpher, H.; Xu, Y.; Sun, L.; Hammarstrom, L. *J. Am. Chem. Soc.* **2005**, *127*, 3855.

JP809122Y